Untangling rain structure from polarimetric GNSS Radio Occultation observables: a 2D tomographic approach

Ramon Padullés, Estel Cardellach & Antonio Rius

Published online: 17 Feb 2017.

Submit your article to this journal ⤤

Article views: 37

View related articles ⤤

View Crossmark data ⤤

Untangling rain structure from polarimetric GNSS Radio Occultation observables: a 2D tomographic approach

Ramon Padullés*, Estel Cardellach and Antonio Rius

Institut de Ciències de l'Espai (ICE - CSIC/IEEC), c/ can Magrans SN,
08193 Cerdanyola del Vallés, Barcelona, Spain
*Corresponding author, e-mail address: padulles@ice.cat

Abstract

A new rain measurement concept will be tested aboard the Low Earth Orbiter (LEO) PAZ, (launch planned for 2016). It aims to detect and quantify intense rain using the polarimetric phase-shift induced by rain droplets along GNSS radio occultation's rays. Due to the integral nature of the measurement, rain intensity and extension are difficult to untangle. The work presented here applies tomographic techniques to reconstruct the precipitation structure from the integrated measurement. The technique shows the capability of retrieving simple structures using only the information self contained in the radio occultation observables, while for more complex structures external information would be needed in order to refine the retrievals.

Keywords: Radio-Occultations, polarimetry, precipitation, tomography.

Introduction

The radio occultation (RO) technique originated in planetary sciences for the study of other planets' atmospheres [Phinney and Anderson, 1968], and measures the phase delay caused by the atmospheric refractivity gradients on the propagation of the radio link. The technique was later adapted to sense the Earth atmosphere using Global Navigation Satellite System (GNSS) signals [e.g. Kursinski et al., 1997, 2000]. GNSS RO space-borne missions, such as GPS/MET [e.g. Rocken et al., 1997], the CHAllenging Minisatellite Payload (CHAMP) mission [e.g. Reigber et al., 2002] and the Formosa Satellite 3 / Constellation Observing System for Meteorology Ionosphere and Climate (FORMOSAT-3/COSMIC) mission [e.g. Anthes et al., 2008], have been proving the Earth's atmosphere since 1995 and nowadays the thermodynamic profiles that they provide are being assimilated operationally into several global numerical weather prediction models (NWP) [e.g. Healy, 2005; Cucurull, 2008]. The use of GNSS RO has become a key component of the operational observing system [National Research Council, 2007].

A new measurement concept has been presented in Cardellach et al. [2015]. It aims to detect and quantify heavy precipitation events using polarimetric GNSS RO, by means of measuring the difference between the phase delays of the horizontal and the vertical

components of the received propagated signal. The study performed in Cardellach et al. [2015] demonstrated not only that heavy rain events could be detected, but also that an approximated vertical structure of the rain cell could be retrieved. The concept has been tested in a field campaign [Padullés et al., 2016] with promising results in views to the spaceborne mission.

One of the limitations of this new concept is the ambiguity between the effect of the rain rate and the effect of the rain cell size, due to the along-path integrated nature of the RO observations. Several solutions are suggested in Cardellach et al. [2015], e.g. the use of the differential signal attenuation, but this is known to be negligible at the frequencies that GPS works (L-band: L1-GPS at 1.575 GHz and L2-GPS at 1.228 GHz).

The solution we suggest in this manuscript is based on a tomographic approach. Tomographic techniques are based on a reconstruction of a cross-sectional imaged object by solving a set of line integrals, obtained from scanning the object from different directions [Herman, 1980]. In this case, the 2 dimensional object that we want to reconstruct is the rain intensity mapped into the RO plane, i.e. the vertical surface where the radio-links are contained. The RO plane is divided into a set of two dimensional voxels. Each voxel is crossed by several consecutive rays with slightly different directions. Therefore, the length of each voxel that is crossed by each ray is different. This allow us to construct a linear set of equations, and the inversion of the rain intensity at each voxel is attempted by solving it. Due to the geometry of the problem, the variety of directions at which voxels are crossed is more restricted than in standard tomographic techniques. For this reason, additional constraints are needed to obtain robust solutions.

Other GNSS applications have used tomographic techniques before, for example Flores et al. [2000] extracted three-dimensional water vapor structures combining observations from several ground stations; or Ruffini et. al. [1998] solved three dimensional ionosphere along RO LEO orbits, combining both RO and ground-based observations. On the precipitation side, there have been some studies that have attempted to reconstruct rain fields using tomographic approaches. For example, Giuli et al. [1991] and Zinevich et al. [2008] used the single path microwave attenuation from network communications, and Moscatelli and Levy [2014] used SAR backscattered measurements to reconstruct the three dimensional rain rate structure. To our knowledge, the approach presented here represents the first attempt to apply the tomographic technique to reconstruct the rain intensity distribution in the propagation plane, from a single RO event. This technique has potential to be applied to other RO applications that require along-ray resolution.

This manuscript presents the technique and it provides an initial assessment of its performance based on simulated signals. The manuscript is structured as follow: In Section "Technique" the technique is introduced, and the required simplifications and constraints are discussed. In Section "Simulation examples" we present the performance of the technique on idealized and non necessarily realistic rain structures, and finally in Section "COSMIC - TRMM collocation simulations" the technique is applied to 259 realistic rain scenarios, obtained from the Tropical Rainfall Measurement Mission (TRMM) and artificially collocated with RO events. The inversion of the simulated polarimetric retrieval that these rain cells would have induced has been attempted with different success, depending on the nature of the rain cell structures. The results are discussed in Section "Discussion".

Technique

Theoretical background

As described in Cardellach et al. [2015], the polarimetric phase shift induced by rain droplets is the result of a cumulated effect along the ray path. In its integral form, it is described by:

$$\Delta\phi = \int_L K_{dp}\ dl \quad [1]$$

where K_{dp} is the specific polarimetric differential phase shift in mm/km, and L is the length along the path (the GNSS community tends to express phase delays in units of length through the electromagnetic wavelength $\lambda : \phi_{length} = \frac{\phi_{rad}}{2\pi}\lambda$). K_{dp} is a function of the forward scattering amplitude ($f_{h,v}$) and $N(D)$, the Drop Size Distribution (DSD). It also depends on the canting angle, which accounts for the misalignment between the local vertical and the drop symmetry axis, and it is defined here as the angle between the propagation line and the local horizontal. The misalignment reduces the polarimetric effect. A complete description of the variables K_{dp}, $f_{h,v}$, and $N(D)$ and the relations among them can be found in e.g., Bringi and Chandrasekar [2001].

Therefore, in a polarimetric RO event our observable is a set of $\Delta\phi$ as a function of each ray tangent point's height (h_{tp}). Our aim here is to untangle the along-ray integrated rain information provided by $\Delta\phi(h_{tp})$ using tomographic techniques.

In order to apply the tomographic approach, we need to discretize the problem and create a grid of voxels. Each voxel has the same area and we will try to retrieve the mean rain intensity within its boundaries. The choice of the voxel's size defines the resolution of the tomographic solution. In Figure 1 there is a visual representation of the voxels and the ray's geometry.

For each ray-i of the radio-occultation, we obtain a polarimetric differential phase shift, $\Delta\phi_i$. This is modelled as the sum of the contribution of the K_{dp} corresponding to each voxel-j times the length that this ray crosses that voxel, L_i^j :

$$\Delta\phi_i = \sum_j L_i^j K_{dp}^j \quad [2]$$

where:

$i = 1, …,$ number of rays;

$j = 1, …,$ number of voxels.

With this configuration, we end up with a linear problem of the form:

$$\mathbf{d} = \mathbf{G\ m} \quad [3]$$

where $\mathbf{d}$ is an array of observed $\Delta\phi_i$, typically of dimension ~1300 (approximate number of rays of radio-occultation observations performed normally at 50 Hz in the lower

troposphere), **G** is the contribution matrix of elements (i.e. the data kernel), and **m** is the array of K_{dp}, the unknowns to be inverted. We use a grid with a resolution of ~ 9.5 km in the horizontal direction and ~250 m in the vertical for the K_{dp} space, which comes determined by the TRMM data: the horizontal resolution corresponds to two times the TRMM one, and the vertical resolution is the same as in the TRMM products. The fact that the retrievals are checked against TRMM data and the computation time are the two main criteria in choosing the resolution.

We need then to solve the linear problem described in Equation [2] using the least squares criterion [e.g. Tarantola, 2005]:

$$\mathbf{m} = \left(\mathbf{G}^{\mathbf{T}}\mathbf{G}\right)^{\mathbf{-1}}\mathbf{G}^{\mathbf{T}}\mathbf{d} \quad [4]$$

Simplifications and constraints

In order to ensure that Equation [4] has a solution, and that is as close as possible to the true one, we have to make some simplifications and apply some constraints to the system. The simplifications relate to the RO plane and are the following:

Simplification 1.   To align all the rays in order to have the tangent point at the same position on the horizontal axis. Figure 1 - panel b shows this simplification.

Simplification 2.   To invert only half of the radio-occultation plane, i.e. the part of the rays from the GPS (or the LEO) to the tangent point. Figure 1 - panel d shows this simplification.

The RO plane it is not a vertical plane, but it is a surface defined by the positions of the GPS and the LEO at each time. Therefore, it implies a slant scanning of the rain, rather than vertical. Forcing each ray to have the tangent point aligned in the horizontal dimension restricts the movement of the tangent point to one dimension, although the true movement is in two dimensions (latitude and longitude). The error that the first simplification is adding to the retrieval depends on the movement of the tangent point. In the cases used in this work, the projection of the movement into one dimension is smaller than the resolution of the technique. However, depending on the RO geometry there can be cases where the tangent point movement is large [Foelsche et al., 2011] and the first simplification could be adding errors.

The second simplification is a critic one. The reason why it has to be applied is the geometrical symmetry between the **G** elements on either side of the tangent point. Due to the spherically symmetric atmosphere assumption (see Section "Ray-tracer"), the rays are identical at both sides of its tangent point, and this geometrical feature would lead to a non-invertible system. What we suggest is to solve the system assuming that only one half of the RO plane exists. Since the observable ($\Delta\phi(h_{tp})$) is anyway scanning the whole ray, the solution will include the rain information from both plane halves in the retrieved half-plane (folded solution). That is, we solve the size and intensity of the precipitation cells but the solution has mirror-ambiguity with respect to the tangent point. Thus, at a first approximation, the solution will only tell the distance at which the rain cells are from the tangent point. This is sketched in panels c) and d) in Figure 1: in panel c) there is a

representation of two rain structures, and in panel d) the retrieved structures affected by the mirror-ambiguity.
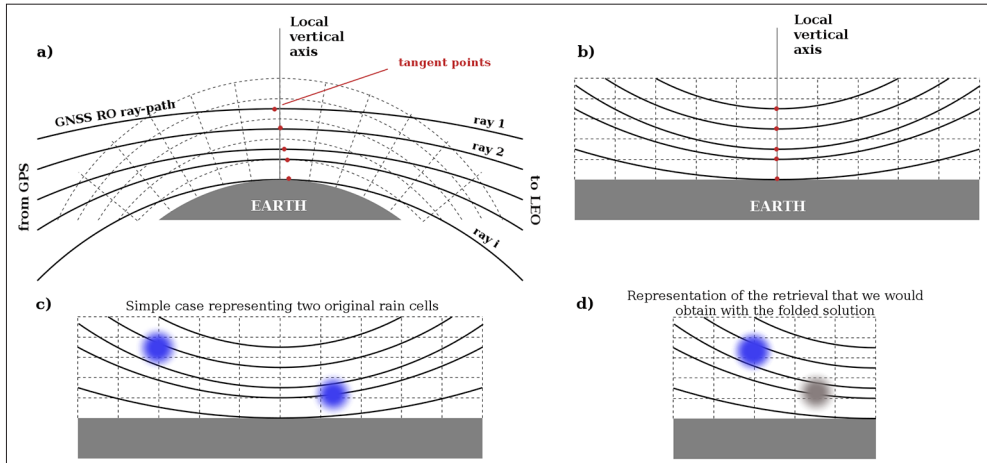
Figure 1 - Sketch of the tomographic approach across the propagation plane. Only a few rays are displayed for clarity purposes. (a) Representation of the geometry of the rays and the voxels. (b) Same as in the (a) panel, but represented as a function of the local altitude and along-ray angular distance to the tangent point. Also, simplification 1 from Section "Simplifications and constraints" has been applied here. (c) Theoretical representation of two rain structures superimposed in the RO plane, and in (d) the retrieval that would be obtained with the tomographic technique. It is shown how, due to the folded solution, the two rain structures shown in (c) are obtained in the left half of the RO plane. In blue, the rain structure that is retrieved in its original position, and in grey the rain structure retrieved in a symmetrical position but in the opposite half of the RO plane (mirror ambiguity).

The main constraint that we apply to help the invertibility of the system is the clustering of the rain voxels:

- Each voxel intensity is assumed to be a linear combination of its surrounding voxels intensities:

$$m_{ij} = \frac{1}{4}\left(m_{i+1,j} + m_{i,j+1} + m_{i-1,j} + m_{i,j-1}\right) \quad [5]$$

This condition forces a smooth behavior of the rain cells with respect of the surroundings. This constraint reduces the degrees of freedom of the system and yields more robust solutions.

Note that both the simplifications and the constraints could benefit from external information, such as meteorological models. This would require a dedicated study not covered in this manuscript, which is focused on a first attempt to apply 2-D tomographic techniques for individual RO events. If the technique is shown to have a good performance with stand-alone information, taking into account the aforementioned limitations, further analysis

could be made using forecast models information. This could help on distinguishing among contributions coming from different areas mapped into the single RO plane half, according to the probability of precipitation, for example.

After applying the simplifications and the constraint, we invert the system with a two-step procedure. First, a regularization method called Truncated Single Value Decomposition (TSVD) [Hansen, 1987] is used. This method increases the stability of the solution with respect to the standard one by removing the smallest eigenvalues. Otherwise, tiny modifications of the input could induce big changes in the output, leading to unrealistic solutions. At this point, we define two more constraints:

- The rain intensity solution obtained with the TSVD method is used to define a mask: those voxels with an intensity above a certain threshold are candidates to hold rain, while the rest are assumed not to contain any rain in it;
- We neglect those voxels placed in the lowest and closest to the tangent point areas in the RO plane, if their retrieved rain intensity is much higher than those placed right above them. The reason is that the lowest rays of the radio-occultation tend to introduce an overestimation of the rain intensity in the area closest to the tangent point. This happens when the radio-occultation is less dense in the lowest part, in terms of number of rays. So, the remaining voxels are added to the previously defined mask.

With the first step we have constrained the rain to certain voxels, so we have reduced significantly the K_{dp} space. It is now possible to proceed with the second step by solving directly Equation [4] (no further constraints) within this reduced space of unknowns.

Ray-tracer

In order to create the grid and fill the matrix **G**, we need the path that the radio-occultation rays have followed. We do not have this information, but we can estimate it using a ray-tracer. Ray tracers are tools that simulate the electromagnetic wave propagation and the path that follows in the propagating medium, accounting for the changes in the refractive index. The ray-tracer that we have used is called Occultation Analysis Tools (OAT) and solves the trajectory of the ray across an atmosphere characterized by a given refractivity vertical profile [Aparicio and Rius, 2004]. The refractivity vertical profiles are standard retrievals of the RO technique, and are obtained under the assumption of no horizontal refractivity gradients (spherically symmetric atmosphere). The same assumption is made by most of the RO atmospheric ray tracers.

Refractivity profiles are provided by several research centers that process and distribute radio occultation data at a near real time. The profiles that we use are the ones contained in the *atmPrf* files provided by University Corporation for Atmospheric Research (UCAR, USA), and available from the UCAR COSMIC Data Analysis and Archival Center (CDAAC) (cdaac-www.cosmic.ucar.edu). We use them as input of the ray tracer. These files contain the refractivity profiles retrieved from the FORMOSAT-3/ COSMIC mission. Refractivity profiles will also be obtained with the PAZ mission, with no need of external information, since PAZ will be able to provide the standard thermodynamic products in addition to the polarimetric ones [Cardellach et al., 2015].

If the paths of the RO rays were parallel among them the technique would not work. However, due to vertical gradients in the atmospheric refractivity, the rays follow slightly different trajectories at different altitudes, even if they are close in time. Each ray is crossing nearby regions of the atmosphere with slightly different geometries, i.e. directions, what makes the tomographic approach to work.

Simulation examples

In this section we want to show the performance of the technique on idealized simulated scenarios. To do so, only one half of the RO plane is used to simulate both the source of the observable and the retrieval. Three different sources are simulated. The three of them represent rain, as given by the K_{dp}. The distribution of the K_{dp} is simulated as a two dimensional Gaussian, that is mapped into the simulated GNSS signals. For each case, the magnitude of the K_{dp}, its size and its position is different. The integral measurement along the rays is the observable $\Delta\phi(h_{tp})$, defined in Equation [1]. The three cases are shown in Figure 2 - left column, and their respective observables are shown in Figure 2 - right column.

The three different cases are thought to have one thing in common: they all produce an observable that has a maximum around the same tangent's point height and the same approximate magnitude. Thus, despite they are placed at three different locations, one observer could not distinguish which one is closer to the tangent point, or which one is placed at a higher altitude, by only looking at the $\Delta\phi(h_{tp})$ profile. The same way, one cannot tell either if the contribution to the observable peak comes from a concentrated intense point or a sparse distribution of light rain.

We show in Figure 3 the result of applying the tomographic approach, following the method explained in Section "Technique", to the observables in Figure 2 - right panel. The conclusions one can obtain from the results in Figure 3 are the following.

Qualitatively, the results of the tomographic approach provide more information and of greater value than the $\Delta\phi(h_{tp})$ alone. The retrieval of the three different cases associate the observable to a concentrated region of rain, and in addition the sources are placed correctly, i.e. the first one is at a higher altitude than the rest, and the second one is placed at a higher altitude than the last one. Similarly, with the horizontal distance to the tangent point.

Quantitatively, the error of the retrieved height of the source is smaller than 1 km, while it ranges from 10 to 50 km in the horizontal dimension. Regarding the magnitude of the K_{dp}, the relative difference between the simulated and the retrieved one is less than a 10% in the first two cases, while in the third case the retrieved magnitude is two times the simulated one. Differences in the retrieved magnitude are directly related with differences in the retrieved size: when the source is overestimated in size, the intensity is underestimated, and vice versa.

The technique definitely shows an improvement of the $\Delta\phi(h_{tp})$-alone observable providing approximate positions and structure of the sources, for the simple simulated cases shown here. It also shows potential for the fully characterization of the rain for certain simple cases. In the next section we apply the same method to real rain scenarios, in order to check the performance in realistic cases.
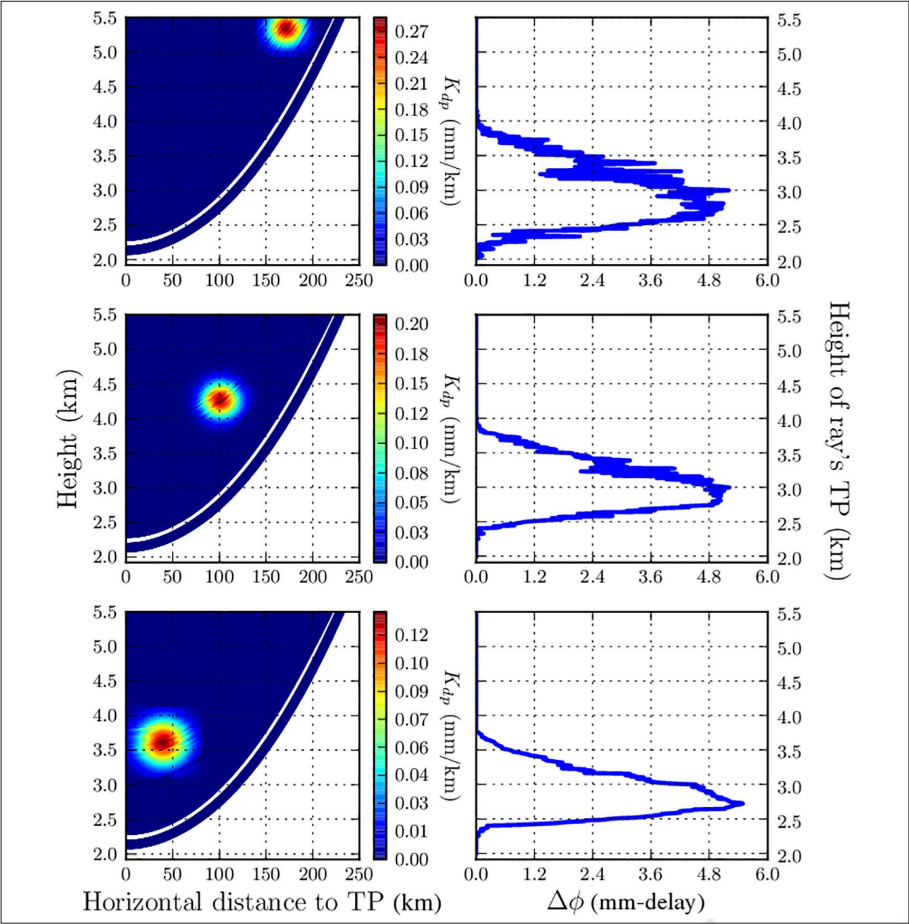
Figure 2 - Simulated precipitation clouds with similar rain structures placed in different heights and locations across the tomographic plane. (Left) The traced RO rays and the interpolated K$_{dp}$ at each ray-point are shown. The density of rays corresponds to an actual RO observation, which typically scans the lower troposphere with more than 1000 rays. (Right) The corresponding observables, $\Delta\phi_p$, as a function of each ray's tangent point altitude.
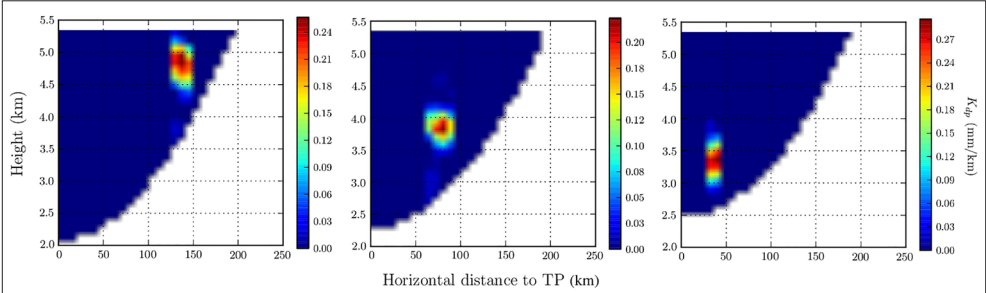
Figure 3 - The recovered rain structures from the simulated observations in Figure 2 using the tomographic approach.

COSMIC-TRMM collocation simulations

In order to test the technique in real rain conditions, we have used real rain products from TRMM for different days, seasons and geolocations. The used TRMM products are the 3 dimensional combined rainfall profiles 2B31 (data and documentation available at http://trmm.gsfc.nasa.gov). We have looked through several TRMM orbits for heavy rain events, and these cases have been artificially collocated with a set of radio occultation rays, simulating an intersection between a RO event and a heavy rain cell. The total number of analyzed events is 259. Again, only half of the RO plane has been used for this analysis. Once the collocations are done, we proceed following the steps described below:

- The TRMM measured rain rate is interpolated into the RO plane;
- We convert the rain rate to K_{dp} as it is explained in Cardellach et al. [2015], so we have the actual K_{dp} at each point of the RO rays;
- We obtain $\Delta\phi(h_{tp})$ using Equation [1];
- Finally, the tomographic approach is applied and the results are examined.

Quantitatively, three aspects of the rain can be efficiently characterized: the position of the peak, the extension of the rain cell, and its intensity. The position of the peak is defined as the location of the point with the highest K_{dp} in the RO plane, i.e. its horizontal distance to the tangent point and its height. The extension of the rain cell is defined as the horizontal and vertical size of the region containing values of K_{dp} larger than the 60% of the maximum. And the intensity is taken as the maximum value of the K_{dp} for each case. These quantities are obtained for both the actual TRMM rain measurements mapped into the RO half-plane and for the retrieval, and are then compared. The results for the position, extension and intensity differences are shown in Figure 4.

The mean difference in horizontal positions is:

$$\left\langle X_{TRMM} - X_{\text{tomo}} \right\rangle = 18.2 \pm 35.1 \, km$$

and the mean difference in height is:

$$\left\langle Y_{TRMM} - Y_{\text{tomo}} \right\rangle = 10.22 \pm 0.56 \, km.$$

For the extension of the rain cells, the mean difference in the horizontal is:

$$\left\langle Lx_{TRMM} - Lx_{\text{tomo}} \right\rangle = -17.94 \pm 19.19 \, km$$

and in height it is:

$$\left\langle Ly_{TRMM} - Ly_{\text{tomo}} \right\rangle = -0.41 \pm 0.54 \, km.$$

The retrieval tends to place the rain closer to the tangent point than it actually is, and tends

to yield a larger rain structure than the original one, especially in the horizontal direction. There are two explanations for this trend. In the first place, the horizontal resolution is large (~ 9.5 km), thus the extension of the small rain cells is easily overestimated. The second reason is the clustering constraint, which mixes and blurs the voxels' solutions. This effect is particularly strong when the original rain is not close together but it has several columnar sub-structures. Then it is more difficult for the technique to resolve the columns individually, and tends to result in a joint and fainter rain cell. Moreover, the errors in the extension determination of the rain cells induce an error in the intensity retrieval as mentioned in the previous section. However, multi-columnar structures have also been correctly solved in certain cases as is shown in Figure 5.
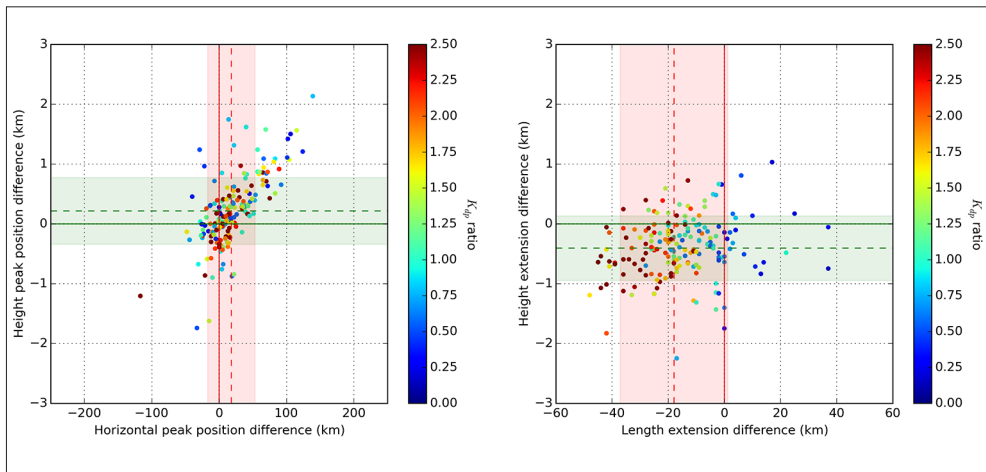

Figure 4 - Statistical results for the simulated collocation between RO and real TRMM rain profiles: (left) The results for the rain cell peak position difference between the original and the retrieved one (X_{TRMM}-X_{tomo}). The solid red and green lines show the zero lines, while the dashed lines show the mean in the horizontal and vertical axis respectively. The shadowed green / red areas show the standard deviation of the means. The color scale shows the K_{dp} ratio between the original and the retrieved rain cell peak. (right) The same as in the left panel but for the rain cell extension.

In Figure 5 there is shown the original and the retrieved rain for 8 cases. For the first four panels (a to d), the retrieval has captured well enough the structure of the rain. Cases e and f show how the retrieval algorithm can blur multi-columnar rain structures and how the rain tends to be retrieved as a fainter and more homogeneous structure than it actually is. The last two cases, g and h, show two examples where the retrieval is not working well, failing to capture the structure and the position of the rain. The proportion of cases in Figure 5 aims to be a fair representation of the 259 cases, evaluated in terms of how the structure of the rain is captured by the tomographic technique.
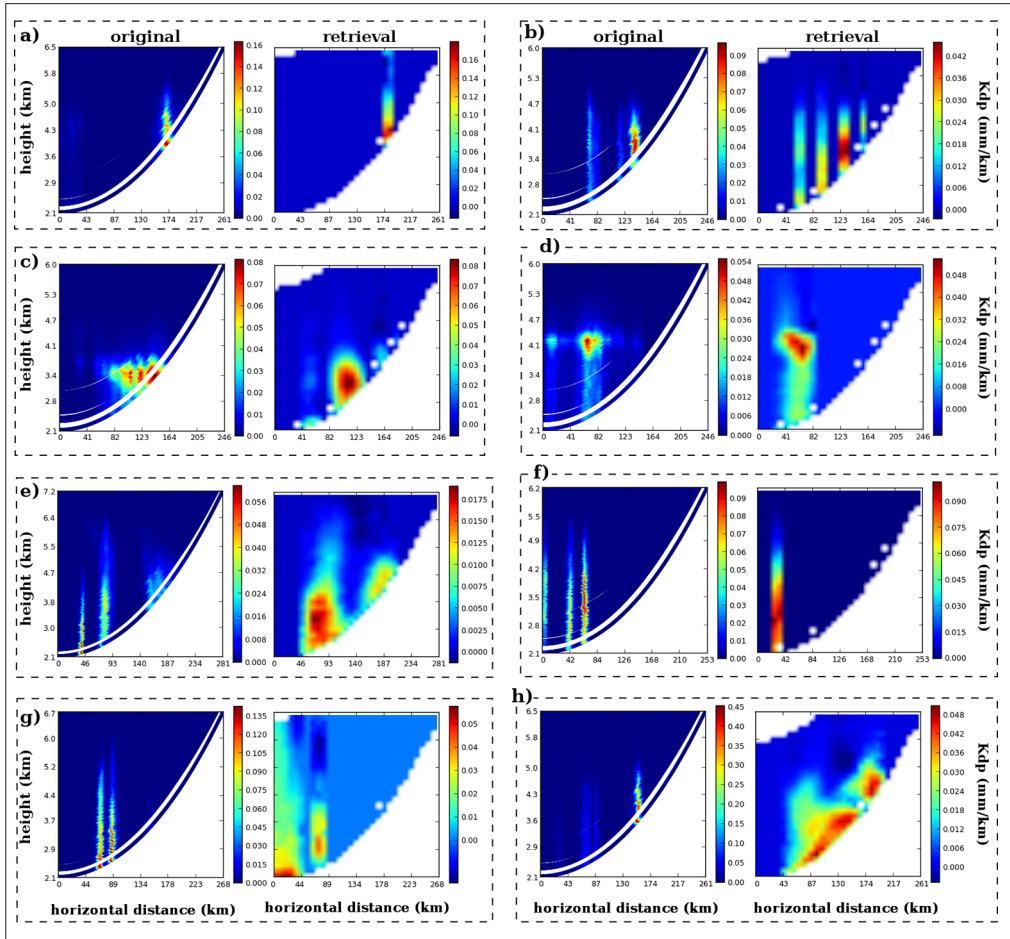
Figure 5 - Examples of the retrievals for different rain cases. Each block represents the original TRMM rain cells (left), and the retrieved solution with the tomographic approach (right). The 8 different cases intend to be a fair representation of the 259 studied cases, in terms of how the structure of the rain is reconstructed with respect the original one.

In terms of analyzing the practical application of this technique into the PAZ experiment, we have to take into account that the RO provided refractivity profiles are mainly contributed by the region within ±100 km around the tangent point [Kursinski et al., 2000]. Therefore, if one wants to relate the measured thermodynamic state to precipitation, the first step is to know if the main part of the detected precipitation is within the influence range. In Figure 6 there are two histograms showing the retrieved peak distances to the tangent point, for the cases where the original rain cell is within a distance of 100 km from the tangent point and for the cases where the original rain cell is further than 100 km from the tangent point. It can be seen how more than 80% of the cases are well placed within this region when the original one is inside. Only less than 10 % are placed closer than 100 km from the tangent point when the original peak is not.
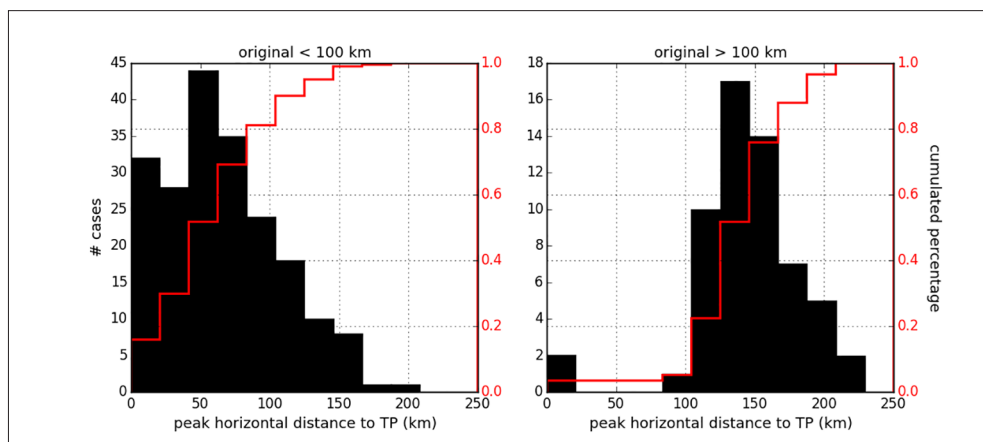
Figure 6 - Left: histogram for the horizontal distance to the tangent point for the cases where the original peak is actually located within 100 km from the tangent point. Right: the same histogram, but for the cases where the original peak is placed further than 100 km from the tangent point. The red line is the cumulated percentage of cases, ruled by the right axis.

Discussion

This study has presented the first attempt to apply a 2D-tomographic approach to untangle the precipitation structure in polarimetric-RO observations across the propagation plane.

The nature of the anticipated polarimetric products of the PAZ mission ($\Delta\phi(h_{tp})$), together with the complex geometry of the radio occultation ray trajectories (due to the vertical refractivity gradients) make the upcoming experiment well suited in order to test this approach.

The main achievement made has been to map the one dimensional observable $\Delta\phi(h_{tp})$ into the 2 dimensional RO observation plane for idealized rain cells. It has been shown how that this technique is able to distinguish similar observed features (e.g. similar $\Delta\phi$ maximum's height) into very different positions of the rain cells that induced the observables.

When we have applied the technique to actual rain cells (measured by TRMM), we have observed bigger errors than in the theoretical cases. The technique tends to place the retrieved rain cells too close to the tangent point, and in terms of extension, it tends to overestimate the size. In turn, overestimation of the extension results in underestimation of the rain intensity.

The obtained errors and standard deviations are big for an observing system, but far from competing with other precipitation observing systems, this technique aims to improve the polarimetric retrievals that the PAZ mission will provide, transforming the one dimensional products to a two dimensional ones. Furthermore, we have shown the capability of the tomographic technique to distinguish between the rain events within 100 km radius from the tangent point and those placed further. This information is of great importance, since will allow us to identify which rain events can be linked with the standard thermodynamic products that will be also provided by PAZ.

As a first demonstration exercise, in this study we have used only information that could be provided by our own satellite (refractivity profiles and the $\Delta\phi(h_{tp})$ observable). Furthermore,

the technique performance has room for improvement and the use of external information must be considered in order to improve the results. For instance, high resolution weather models could be used, so the tomographic retrieval follows a variational (2D-VAR) approach. The use of a model could have a direct impact in one of the weakness of the technique: the simplifications and constraints defined in Section "Simplifications and constraints". With the use of the model, instead of using only one half of the plane, one could use a predicted quantity, (for instance, the relative humidity) as a first guess solution of the least squares system. This would break the symmetry between the two halves of the RO plane, and would increase the robustness of the solution. This and additional studies on the improvement of the technique are left for future research.

Acknowledgements

References

Anthes R., Bernhardt P.A., Chen Y., Cucurull L., Dymond K.F., Ector D., Healy S.B., Ho, S.P., Hunt D.C., Kuo Y.H., Liu H., Manning K., McCormick C., Meehan T.K., Randel W.J., Rocken C., Schreiner W.S., Sokolovskiy S.V., Syndergaard S., Thompson D.C., Trenberth K.E., Wee T.K., Yen N.L., Zeng Z. (2008) - *The COSMIC/FORMOSAT-3 Mission, Early Results*. Bulletin of the American Meteorological Society, 89 (3): 313-333. doi: http://dx.doi.org/10.1175/BAMS-89-3-313.

Aparicio J.M., Rius A. (2004) - *A raytracing inversion procedure for the extraction of the atmospheric refractivity from GNSS travel-time data*. Physics and Chemistry of the Earth, Parts A/B/C, 29 (2-3): 213-224. doi: http://dx.doi.org/10.1016/j.pce.2004.01.008.

Bringi V., Chandrasekar V. (2001) - *Polarimetric weather radar; principles and applications*. Cambridge University Press. doi: http://dx.doi.org/10.1017/CBO9780511541094.

Cardellach E., Tomás S., Oliveras S., Padullés R., Rius A., de la Torre-Juárez M., Turk F.J., Ao C.O., Kursinski E.R., Schreiner B., Ector D., Cucurull L. (2014) - *Sensitivity of PAZ LEO Polarimetric GNSS Radio-Occultation Experiment to Precipitation Events*. IEEE

Transactions on Geoscience and Remote Sensing, 53 (1):190-206. doi: http://dx.doi.org/10.1109/TGRS.2014.2320309.

Committee on Earth Science and Applications from Space: A Community Assessment and Strategy for the Future (2007) - *Earth Science and Applications from Space: National Imperatives for the Next Decade and Beyond*. The National Academies Press, 454p. doi: http://dx.doi.org/10.17226/11820.

Cucurull L., Derber J.C. (2008) - *Operational Implementation of COSMIC Observations into NCEP's Global Data Assimilation System*. Weather and Forecasting, 23 (4): 702-711. doi: http://dx.doi.org/10.1175/2008WAF2007070.1.

Flores A., Ruffini G., Rius A. (2000) - *4D tropospheric tomography using GPS slant wet delays*. Annales Geophysicae, 18: 223-234. doi: http://dx.doi.org/10.1007/s00585-000-0223-7.

Foelsche U., Syndergaard S., Fritzer J., Kirchengast G. (2011) - *Errors in GNSS radio occultation data: Relevance of the measurement geometry and obliquity of profiles*. Atmospheric Measurement Techniques, 4: 189-199. doi: http://dx.doi.org/10.5194/amt-4-189-2011.

Giuli D., Toccafondi A., Gentili B., Freni A. (1991) - *Tomographic Reconstruction of rainfall fields through microwave attenuation measurements*. Journal of Applied Meteorology, 30 (9): 1323-1340. doi: http://dx.doi.org/10.1175/1520-0450(1991)030<1323:TRORFT>2.0.CO;2.

Hansen P.C. (1987) - *The truncated svd as a method for regularization*. BIT Numerical Mathematics, 27 (4): 534-553. doi: http://dx.doi.org/10.1007/BF01937276.

Healy S.B., Jupp A.M., Marquardt C. (2005) - *Forecast impact experiment with GPS radio occultation measurements*. Geophysical Research Letters, 32 (3): L03,804. doi: http://dx.doi.org/10.1029/2004GL020806.

Herman G.T. (1980) - *Image Reconstruction from Projections.* The Fundamentals of Computerized Tomography, New York - London Academic Press, XII. doi: http://dx.doi.org/10.1002/zamm.19830630227.

Kursinski E.R., Hajj G.A., Schofield J.T., Linfield R. P., Hardy K.R. (1997) - *Observing Earth's atmosphere with radio occultation measurements using the Global Positioning System*. Journal of Geophysical Research, 102 (97): 23.429-23.465. doi: http://dx.doi.org/10.1029/97JD01569.

Kursinski E.R., Hajj G.A., Leroy S., Herman B. (2000) - *The Radio Occultation Technique*. Terrestrial, Atmospheric and Oceanic Sciences, 11 (1): 53-114.

Moscatelli M., Levy G. (2014) - *Three dimensional reconstruction of rain rates from X-SAR measurements using tomography*. Proceedings of 12th Biennal Conference of Pan Ocean Remote Sensing Conference (PORSEC 2014): 151-162.

Padullés R., Cardellach E., de la Torre Juárez M., Tomás S., Turk F.J., Oliveras S., Ao C.O., Rius A. (2016) - *Atmospheric polarimetric effects on GNSS Radio Occultations: The ROHP-PAZ field campaign*. Atmospheric Chemistry and Physics, 16: 635-649. doi: http://dx.doi.org/10.5194/acp-166352016.

Phinney R.A, Anderson D.L. (1968) - *On the radio occultation method for studying planetary atmospheres.* Journal of Geophysical Research, 73 (5): 1819-1827. doi: http://dx.doi.org/10.1029/JA073i005p01819.

Reigber C., Lühr H., Schwintzer P. (2002) - *CHAMP mission status.* Advances in Space

Research, 30 (2): 129-134. doi: http://dx.doi.org/10.1016/S0273-1177(02)00276-4.

Rocken C., Anthes R., Exner M., Hunt D., Sokolovskiy R., Ware R.H., Gorbunov M., Schreiner W., Feng D., Herman B.M., Kuo Y.H., Zou X. (1997) - *Analysis and validation of GPS/MET data in the neutral atmosphere*. Journal of Geophysical Research, 102: 29849-29866. doi: http://dx.doi.org/10.1029/97JD02400.

Ruffini G., Flores A., Rius A. (1998) - *GPS tomography of the ionospheric electron content with a correlation functional*. IEEE Transactions on Geoscience and Remote Sensing, 36 (1): 143-153. doi: http://dx.doi.org/10.1109/36.655324.

Tarantola A. (2005) - *Inverse problem theory and methods for model parameter estimation*. Society for Industrial and Applied Mathematics. doi: http://dx.doi.org/10.1137/1.9780898717921.

Zinevich A., Alpert P., Messer H. (2008) - *Estimation of rainfall fields using commercial microwave communication networks of variable density*. Advances in Water Resources, 31 (11): 1470-1480. doi: http://dx.doi.org/10.1016/j.advwatres.2008.03.003.